The influence of CO_2 mixture composition and equations of state on simulations of transient pipeline decompression

Aursand, E., Aursand, P., Hammer, M., Lund. H.

SINTEF Energy Research, Sem Sælands vei 11, NO-7034 Trondheim, Norway

Abstract

In a CO_2 transport pipeline, decompression can occur either due to planned maintenance or accidental rupture. We investigate the impact of modelling simplifications and assumptions regarding the purity of CO_2 on the decompression of an industrial scale transport pipeline. Using industrially relevant compositions of impurities we both calculate simplified (isentropic) decompression curves as well as perform full-scale fluid simulations using models for heat transfer, friction and choked flow. Herein, we compare the use of the Peng–Robinson cubic equation of state (EOS) with the use of the highly accurate EOS-CG and GERG-2008 EOS.

We find that the saturation pressure can change significantly when certain impurities are present, even when in small quantities. A simplifying assumption that CO_2 is pure can therefore lead to significant underestimation of the fluid pressure during the decompression, with consequences for the prediction of running ductile fractures. The choice of EOS was found to mainly affect the velocities of the initial decompression wave, with the long-time evolution of the pipeline decompression remaining relatively unchanged. The temperature minimum did neither depend significantly on the choice of EOS nor the presence of impurities.

Keywords: CO_2 transport, impurities, pipeline decompression, running ductile fracture

1. Introduction

CO_2 transport is a key component in a carbon capture and storage (CCS) infrastructure. Pipelines are often a cost-efficient solution for onshore transport and short-distance or high-volume offshore transport. CO_2 is most efficiently transported in its liquid or supercritical form, which implies high operating pressures, of the order of 100 bar. Although CO_2 has been transported and used for enhanced oil recovery in the United States for several decades [1], CO_2 in a CCS infrastructure will likely be different due to other impurities [2]. It is therefore necessary to develop new and accurate models for thermodynamics and pipeline flow of CO_2 mixtures typical for CCS.

In a CO_2 transport system, depressurization may occur, either intentionally for shutdown or maintenance, or by accident due to leakage through a damaged section of the pipeline. In the event of such a rapid depressurization/expansions, a fluid will experience a decrease in temperature due to *isentropic expansion*. Additionally, as gas escapes the pipeline, the

liquid boils to fill the vacant volume, absorbing the needed latent heat in the process. When these temperature reducing effects are able to overcome the rate of heat transfer from the surroundings, we have what is called *auto-refrigeration*. Eventually, when all of the liquid has vaporized, and most of it has escaped the pipeline, the heat transfer from the surroundings will make the temperature start to increase again. The above implies that there is a certain minimum temperature occurring in the pipeline at some location and time. It is of interest to predict this lowest temperature for various safety reasons, including ensuring operation above the ductile–brittle transition temperature (DBTT) of the pipeline steel [3], especially at welds. Failing to stay above the DBTT introduces a risk of brittle fractures in the pipeline. Low temperatures can also cause the formation of ice and hydrates which may plug the pipe, or be outside the temperature design specifications of equipment such as pumps and valves. Additionally, a rapid temperature decrease may also be demanding on materials and equipment.

Even well above the DBTT and hydrate-forming temperatures, *running ductile fracture* [4] is another safety concern. If there for some reason is a small initial fracture, from e.g. corrosion or an accidental outside impact, the high pressure inside the pipeline may drive this fracture to grow rapidly along the pipeline at speeds in the region of 100–200 m/s. Designing a pipeline to avoid that this fracture grows indefinitely, i.e. ensuring *fracture arrest*, is called *fracture propagation control*. Central to this analysis is the concept of the *fracture race*, which is a race between the running fracture and the speed at which pressure levels propagate through the pipeline. This decompression speed is mainly governed by the speed of sound. As opposed to natural gas, CO_2 in pipelines will encounter a phase transition (boiling) if decompressed. When the saturation point (i.e. the bubble point) is reached, the speed of sound drops rapidly. Within equilibrium approximations, this is represented by a discontinuity. This discontinuity leads to a growing pressure plateau in the pipeline, at the saturation pressure. The front of the plateau propagates with the liquid decompression speed, and the rear propagates with the two-phase decompression speed.

The central issue in fracture propagation control is to ensure that the two-phase decompression speed is faster than the fracture speed at the saturation point. If so, the fracture will fall behind the high pressure plateau, and arrest. This reveals two central thermodynamic parameters: The saturation pressure, and the two-phase decompression speed at the saturation point. Both of these may be affected by impurities, and in terms of modelling, the choice of thermodynamic model (EOS).

CO_2 transported by pipeline is rarely 100% pure [5], especially not when coming from capture processes in a Carbon Capture and Storage (CCS) system. The presence of impurities will significantly influence the thermodynamic behaviour of the fluid compared to pure CO_2 [6], and may thus be expected to influence both the temperatures reached by auto-refrigeration, and the pressure and speed of sound at the saturation point.

The presence of impurities requires delicate treatment of the thermodynamic calculations involved in simulations. However, when choosing equations of state, there is an ever-present trade-off between accuracy and efficiency. Reference equations with a small and well-defined error bar exist. Performing certain industrial-scale simulations using such models can result in a detrimental increase in computational cost. It is therefore important to quantify the

effect using classic cubic EOSs has on relevant case studies for transient pipeline decompression.

A number of authors have developed and validated models for depressurization of CO_2 pipelines. Munkejord and Hammer [9] presented both a homogeneous equilibrium model (HEM) and a two-fluid model (TFM), and compared their results to experimental data from a number of experiments [**?** **?** **?**]. Brown et al. [**?**] also consider the effects of non-equilibrium during depressurization. A similar study to the one presented in the current work was performed by Mahgerefteh et al. [**?**], which concerned the effect of friction, heat transfer and impurities on depressurization of CO_2 pipelines. In this work our focus is mainly on the effect of various impurities on depressurization, but our homogeneous equilibrium flow model also includes friction and heat transfer. For running ductile fractures, models that include both fluid and structure modelling have been developed by e.g. Mahgerefteh et al. [**?**] and Nordhagen et al. [**?**]. For a more extensive review of models for CO_2 pipeline depressurization, see e.g. [9**?**].

1.1. Paper outline

In this work, we investigate depressurization of a 5 km pipeline using two different computational approaches. The first approach is based on a pure thermodynamic model, which calculates isentropic decompression from a certain initial state. The second approach uses a two-phase flow model with friction and heat terms to predict the flow during the decompression. Both models are combined with both state-of-the-art and classic cubic thermodynamic models. The main objective of the paper is to quantify the effect the following two simplifications have on the modelling of the depressurization problem:

1. Using a computationally efficient cubic EOS instead of a complex reference EOS
2. Neglecting impurities in CO_2 mixtures from CCS capture processes

The paper is organized as follows: In Sec. 2 we describe the homogeneous equilibrium model for the fluid flow, including models for friction, heat transfer and choked flow out of the pipeline. We also present a simplified model that assumes isentropic flow, which is used to examine a larger number of cases. The two thermodynamic models used in the calculations are also introduced. Sec. 3 presents the CCS relevant cases that will be considered including pipeline dimensions, physical parameters and composition of impurities. Finally, in Secs. 4 and 5 we present results from simulations of the selected cases. Herein, we look at isentropic decompression curves as well as full pipeline simulations. Sec. 6 summarizes the results and outlines further work.

2. The model

The model used to investigate depressurization behaviour of pipelines has been compared and validated to experimental data for pure CO_2 and CO_2-rich mixtures. Drescher et al. [22] compare simulations with experimental depressurization data for three mixtures of CO_2 and N_2. The mixtures contain 10, 20 and 30 mol % N_2, and are simulated using the Peng–Robinson equation of state. The modelled pressure during depressurization are

in fair agreement with the experimental measured pressure. Munkejord and Hammer [9] later simulate the same experimental data, and investigate the influence of the heat transfer model and boundary conditions, and as a result improve the model. The experimental depressurization data from Botros et al. [**?**] of a CO_2 and CH_4 system is also modelled. For this mixture it is seen that GERG-2008 is far superior to Peng-Robinson. The same deficiencies of Peng–Robinson is seen comparing the model with a multi-component mixture depressurization experiment [**?**].

Recently Munkejord et al. [**?**] applied the same model to simulate a pure CO_2 depressurization entering the solid region. Using the Span-Wagner equation of state [**?**], extended with a model for dry ice [23], good agreement with experiments were observed. Using the Span–Wagner equation of state is identical to using the EOS-CG model for pure CO_2.

2.1. The homogeneous equilibrium model

A multi-component homogeneous equilibrium model is solved for the fluid flow in the pipeline. Specifically, we solve equations for the conservation of total mass, momentum and internal energy, given by

$$\frac{\partial \rho}{\partial t} + \frac{\partial (\rho u)}{\partial x} = 0, \tag{1a}$$

$$\frac{\partial (\rho u)}{\partial t} + \frac{\partial (\rho u^2 + p)}{\partial x} = -\tau_{\mathrm{w}}, \tag{1b}$$

$$\frac{\partial E}{\partial t} + \frac{\partial [u(E+p)]}{\partial x} = Q_{\mathrm{w}}. \tag{1c}$$

In the above, ρ is the mixture mass density, u is the mixture velocity, p is the pressure and E is the mixture total internal energy. The terms τ_{w} and Q_{w} represent friction and heat transfer at the pipe wall, respectively.

In this model, the multi-component, multi-phase fluid is assumed perfectly mixed with a common temperature, pressure and velocity. In order to close the system, temperatures and pressures are calculated using equations of state, taking into account the fluid composition. The thermodynamic models are described in detail in Sec. 2.5.

2.2. Friction and heat transfer

The multi-component, two-phase flow is assumed to be perfectly mixed, hence the two phases have the same velocity. For the wall friction τ_{w}, we use the well-established correlation of Friedel [7]. Herein, the relative roughness of the pipe is assumed to be 5×10^{-5}.

The term Q_{w} in Eq. (1c) is the heat transfer rate per volume of fluid, i.e.

$$Q_{\mathrm{w}} = \frac{2}{r_{\mathrm{i}}} h_{\mathrm{i}} (T_{\mathrm{w}} - T) \tag{2}$$

where r_{i} is the inner radius of the pipeline and h_{i} is the inner heat transfer coefficient. In order to obtain the wall temperature T_{w}, a transient model for the conduction through the

pipe and the surrounding soil is used. Specifically, the radially symmetric time-dependent heat equation

$$\rho c_p \frac{\partial}{\partial t} T(r,t) = \frac{1}{r} \frac{\partial}{\partial r} \left(r \lambda(r) \frac{\partial}{\partial r} T(r,t) \right) \tag{3}$$

is solved in two concentric layers around the fluid, as shown in Fig. 1. Herein, c_p is the specific heat and λ is the thermal conductivity.

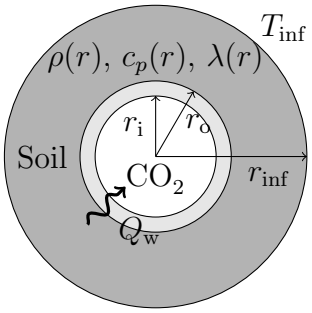

Figure 1: The domain used for the radially symmetric transient heat transfer model.

While the outside (pipe-soil) heat transfer coefficient is assumed constant, the *inner* heat transfer coefficient, h_{i}, is calculated using experimentally fitted correlations. When the flow is single-phase, the standard Dittus–Boelter equation is used when the flow is turbulent, a Nusselt number of 3.66 is used when the flow is laminar, and a linear interpolation between the two is used through the transition regime. When the flow is two-phase, and the wall temperature is higher than the fluid temperature, boiling occurs at the wall. In this case, the Gungor–Winterton correlation in its simplified form [8] is used.

2.3. Outflow model

2.3.1. Choked outflow

The escape of the pressurized fluid through an opening at one end of the pipeline is modelled using steady-state choked-flow theory. The effect of using a steady state and not a dynamic choke condition is discussed by Munkejord and Hammer [9]. The fundamental steady-state choked-flow assumption is that the flow through the full-bore opening is isentropic and follows the Bernoulli principle

$$\frac{1}{2}u^2 + h = \text{constant} \tag{4}$$

along any streamline, where h is the specific enthalpy. The assumption of homogeneous equilibrium is extended to the escape flow, and energy loss due to friction and heat transfer is assumed to be negligible along the escape streamline. The pressure p at the outlet is calculated by looking for solutions to the equation

$$u(p, s_0) = c(p, s_0), \tag{5}$$

where the velocity is given by

$$u(p, s_0) = \left(2\left(h_0 - h(p, s_0)\right) + u_0^2\right)^{1/2}. \tag{6}$$

In the above, c is the speed of sound, and s_0, u_0 and h_0 denote the specific entropy, velocity and specific enthalpy in the pipeline, respectively. Since the speed of sound can be discontinuous when reaching the saturation line, special care must be taken when solving Eq. (5) in cases where the flow speed u falls within this discontinuity. If this happens, the flow is assumed to be choked just inside the two-phase region.

If a solution $p_{\text{choke}} \in [p_{\text{atm}}, p_0]$ to Eq. (5) is found, the escape flow is choked and the pressure at the outlet is set as $p_{\text{e}} = p_{\text{choke}}$. If no such solution is found, the escape flow is subsonic and the outlet pressure is the atmospheric pressure $p_{\text{e}} = p_{\text{atm}}$. Given the outlet pressure, the rest of the outlet properties are obtained using the equation of state at the point (p_{e}, s_0).

2.3.2. Boundary condition

When solving the governing equations Eq. (1), the choked outflow model is used to set a variable boundary condition at the side of the pipeline where the full-bore opening is located. The state just inside the opening is used as the initial streamline state (p_0, s_0, u_0), the choked flow calculation is performed, and the state just outside the opening is then set to (p_{e}, s_0). This difference in state is used to construct fluxes of mass, momentum and energy across the boundary, out of the pipeline.

2.4. Simplification: Isentropic full-bore decompression of an infinite pipe

Under some conditions, the governing equations (1) for a full-bore opening case may be solved in a much simpler way than by computational fluid dynamics. The assumptions are:

- Friction (τ_{w}) and heat transfer (Q_{w}) may be neglected, giving isentropic flow. This essentially gives the homogeneous fluid-dynamic Euler equations.
- The pipeline is infinitely long in the direction away from the full-bore opening. Before the initial pressure wave has propagated to the actual pipeline length, this is a completely accurate approximation, as the pipeline end cannot have an effect on the event before information about the event has reached it.

At a given time in a full-bore decompression event, there will be a pressure profile $p(x)$ in the pipeline. At each point there will also be a flow velocity $u(x)$ towards the opening. It turns out that given the above listed assumptions, one may analyse the characteristics of the Euler equations, to show that these two function are related as [10]

$$\frac{\mathrm{d}|u|}{\mathrm{d}p} = -\frac{1}{\rho c}. \tag{7}$$

The flow speed at a given pressure level is constant in time, and may then be calculated from

$$|u(p)| = \int_p^{p_0} \frac{1}{\rho(p', s_0)c(p', s_0)} \mathrm{d}p'. \tag{8}$$

where $\rho(p, s)$ and $c(p, s)$ can be calculated from an equation of state, taking into account the possible two-phase state.

The speed at which a pressure level moves away from the full-bore opening is then $v(p) = c(p) - |u(p)|$. Note that this is the same as the decompression speed calculated in two-curve models for pipeline running ductile fracture [4]. The pressure at which $v(p) = 0$ is the pressure at the full-bore opening, in this approximation. This state is constant in time, and we call it the choke point. At the choke point, we find the temperature $T(p_{\text{choke}}, s_0)$, which is the lowest temperature encountered in this approximation. We call this the choke temperature T_{choke}.

In this approximation, every fluid element in the decompression event will follow the isentropic path from the common initial state. To simulate the event, we calculate all thermodynamic properties, and flow velocity from Eq. (8), along the isentrope until reaching the choke point. This gives insight into the ranges of temperature and pressure encountered in the event, and when the two-phase state is reached (the saturation point).

2.5. Thermodynamics and thermophysical properties

In this work we consider the classical cubic equation of state (EOS) of Peng and Robinson (PR) [11], and the new Helmholtz state function based EOSs, EOS-CG [12, 13**?**] and GERG-2008 [15]. The Helmholtz state function is expressed in the natural variables temperature and density/volume. Since EOS-CG is in a development stage only a limited number of species are available. Of the species considered in this work, only CO_2, N_2, O_2 and Ar are available. To describe the mixtures completely, GERG-2008 is used to describe the components H_2, CH_4 and C_2H_6. In this work, the model combining EOS-CG and GERG-2008 is termed the EOSCG-GERG equation of state. When investigating if the PR EOS is sufficiently accurate for the applications considered in this work, EOSCG-GERG is used as the more accurate point of reference.

The GERG-2008 and EOS-CG equations of state are constructed in a similar manner, by mixing pure fluid equations of state using Helmholtz free energy mixing rules [16, 17]. While GERG-2008 is developed for description of natural gas, where CH_4 is the main component, EOS-CG is being developed for combustion gases (CG), where CO_2 is the main component. EOS-CG is based on pure fluid reference equation for the Helmholtz free energy, while GERG-2008 uses a simplified version of the pure fluid reference equations. Especially in the critical region, the use of accurate pure-fluid EOSs will give an improvement over GERG-2008. EOS-CG have so far improved binary mixture models and parameters have been developed for the exhaust-gas components CO_2, N_2, O_2, Ar, CO and H_2O. EOS-CG shows significant improvement over GERG-2008 for some mixtures [**?**].

EOS-CG is regressed to available experimental data for vapour–liquid equilibrium (VLE), density, heat capacity, Joule–Thomson coefficient, speed of sound, excess enthalpy, and the second cross-virial coefficient. For the binary systems included, the relative error between model and experimental data is reported to mostly be within 1.0 % for all properties. GERG-2008 have been tuned to similar data, and was recently adopted by ISO as a standard for natural gases (ISO 20765-2/3).

Cubic EOSs can predict VLE quite well, but are known for poor density predictions in the liquid phase and in the critical region. Li and Yan [18] found SRK to predict VLE properties in CO_2 mixtures satisfactorily. In process modelling, this is to some extent overcome using density corrections. For CO_2-rich mixtures there seem to be little improvement using standard density corrections. For fast transients in pipelines, where also the speed of sound comes into play, a density correction is in any case not sufficient. The more detailed modelling approach of EOS-CG/GERG-2008 is far superior [9], as these systems have been regressed against both density and speed-of-sound experimental data.

Dry-ice in equilibrium with liquid and vapour is not considered in this work. Even if a state requiring dry-ice formation is not reached inside the pipeline, dry-ice might be of relevance for the boundary conditions. Using an auxiliary model to describe dry-ice formation [19, 20], is a natural extension of this work.

When evolving Eqs. (1a) to (1c) in time, the density and energy of the system is updated. To determine the temperature, pressure, phase fractions and phase component fractions, the iso-choric–iso-energetic phase-equilibrium problem must be solved.

Also, when calculating transient boundary conditions for Eqs. (1a) to (1c), and when performing the simplified simulations described in Sec. 2.4, the isentropic approximation is used. Both introduce the challenge of finding an equilibrium state given pressure and entropy, the iso-baric–iso-entropic phase-equilibrium problem.

The approaches presented by Michelsen [21] are used to solve these global maximization/minimization phase-equilibrium problems. These methods have successfully been used for depressurization of CO_2 mixtures earlier [22, 9]. To the authors' knowledge, solving the iso-choric–iso-energetic phase-equilibrium problem using EOS-CG or GERG-2008 has not been reported earlier in the literature. In the case of pure CO_2 the approach of Hammer et al. is used [23], when solving the entropy–pressure and energy–density problem.

Fluid mixture viscosity is described by the extended corresponding-principle-state approach TRAPP [24]. TRAPP is also used for thermal conductivity prediction [25].

There is a substantial CPU penalty when running CFD using direct calls to cubic equations of state. Using the more complex GERG-2008 and EOS-CG is associated with an even larger CPU penalty, as the equation is much more complex. At the same time GERG-2008 and EOS-CG use detailed state equations for every component, and combine them using Helmholtz mixing rules, making them scale poorly with the number of components.

A common way to improve the situation is to use tabulated thermodynamic property data [**?**]. However, thermodynamic property tabulation is uncommon for the fluid composition space, and limited to simulations with fixed overall composition. In addition, tabulation introduces error and inconsistency compared to solving the equation of state directly [**?**]. In order to quantify these errors and inconsistencies, simulations using tabulated properties should be compared and validated against the more correct approach used in this work.

3. Case studies

3.1. Composition of impurities

We wish to study the impact of the presence of impurities relevant for CCS on the decompression of a CO_2 pipeline. The impurities that are present will depend both on the source and the specific capture technology used. In this work we compare four relevant compositions, given in Tab. 1. Composition #2, which is typical for amine capture from coal power plants, has only minute quantities of impurities. Conversely, for composition #4, there is a significant presence of methane, as well as smaller quantities of other substances.

	Description	CO_2	N_2	O_2	Ar	H_2	CH_4	C_2H_6
#1	Pure CO_2	100.0%						
#2	Coal power plant, amine capture	99.77%	2000	200	100			
#3	Coal power plant, selexol capture	98.25%	6000		500	1%	1000	
#4	Natural gas processing, amine capture	95%	5000				4%	5000

Table 1: Composition (in mole fraction by % or ppm) of CO_2 mixtures for our case studies. Compositions #2–#4 have been identified by the IMPACTS project [**?**] as typical for CO_2 mixtures captured from coal power plants and natural gas processing. Minor amounts (<0.04%) of NOx, SOx, CO, H_2S, NH_3 and amine have been neglected.

The impact of the amount of impurities (by mole fraction) is of particular interest. Moreover, the physical properties of different impurities typically found in CO_2 vary greatly, meaning that they individually can have a very different effect on the overall mixture. In order to study this, we will also consider a number of binary mixtures of CO_2 and individual impurities.

3.2. Decompression scenario

For the purpose of this work, we consider a scenario where a 5 km long pipe pressurized at 100 bar is vented to the atmosphere through a full-bore opening at one end. The inner diameter of the pipe is 0.1 m and the thickness is 2 cm. The diameter is somewhat smaller than that of a full-scale CO_2 pipeline, but has been chosen to increase heat transfer. This allows us to avoid temperatures below the triple point, which would require a dry ice model, which is not included in our flow simulations. The steel pipe is assumed to be completely buried in soil, a situation relevant both for onshore and offshore CO_2 transport. Herein, the relevant physical parameters are given in Tab. 2. Initially, the fluid is assumed to be stationary and in thermal equilibrium with the pipeline surroundings at a temperature of 20 °C.

Parameter	Symbol	Value
Pipe thermal conductivity	λ_p	$45\,\mathrm{W/(m\,K)}$
Pipe density	ρ_p	$7850\,\mathrm{kg/m^3}$
Pipe specific heat	$c_{p,\mathrm{p}}$	$470\,\mathrm{J/(kg\,K)}$
Pipe thickness	d_p	$2\,\mathrm{cm}$
Soil thermal conductivity	λ_s	$2.0\,\mathrm{W/(m\,K)}$
Soil density	ρ_s	$1800\,\mathrm{kg/m^3}$
Soil specific heat capacity	$c_{p,\mathrm{s}}$	$1000\,\mathrm{J/(kg\,K)}$
Soil thickness	d_s	$98\,\mathrm{cm}$
Outside heat transfer coefficient	h_o	$4.0\,\mathrm{W/(m^2\,K)}$
Outside temperature	T_inf	$293\,\mathrm{K}$

Table 2: Physical parameters for the radially symmetric transient heat transfer model.

4. Isentropic full-bore decompression

Decompression cases based on Sec. 3 were investigated according to the method described in Sec. 2.4. The pressure, temperature, density and speed of sound along the isentropes, at pressures above the choke point, are shown for pure CO_2 (Fig. 2), coal power amine capture (Fig. 3), coal power selexol capture (Fig. 4) and natural gas processing amine capture (Fig. 5).

In pipeline decompression, important parameters include the saturation pressure (p_sat), the lower speed of sound at the saturation discontinuity ($c_\mathrm{sat,low}$), and the lowest encountered temperature (T_choke). These values are shown in Tab. 3.

Composition	p_sat (bar)		$c_\mathrm{sat,low}$ (m/s)		T_choke (°C)	
	PR	EOSCG-GERG	PR	EOSCG-GERG	PR	EOSCG-GERG
#1	47.5	49.5	48.7	50.4	-6.5	-6.7
#2	48.6	50.7	50.3	52.2	-6.5	-6.7
#3	60.3	62.0	71.8	69.5	-5.8	-6.0
#4	59.8	62.4	64.0	65.5	-8.1	-8.0

Table 3: Results for saturation pressure, plateau-rear speed of sound, and choke temperature in the infinite pipe isentropic decompression approximation, for each of the four composition cases defined in Tab. 1.

4.1. Effect of EOS

The two EOSs predict very similar phase envelopes for each case. However, the saturation points are still somewhat different, mostly due to different slopes of the isentropes in the liquid region. Still, they agree closely on the final choke point, not only on temperature and pressure, but also on density and speed of sound. Due to this, they also agree closely on the predicted outflow rate from the pipeline, since $u = c$ on the outflow point.

Overall we may summarize the following regarding the effect of EOS choice:

- PR underpredicts both density and speed of sound in the liquid phase, as compared to EOSCG-GERG.
- PR slightly underpredicts ($\approx$ 2–3 bar) the saturation pressure (p_{sat}) of the isentropes, as compared to EOSCG-GERG.
- The EOSs agree well on the lower speed of sound at the saturation discontinuity ($c_{\text{sat,low}}$).
- The EOSs agree well on the extent of the phase envelope.
- The EOSs agree well on the choke point, and thus the lowest temperature occurring in the decompression in this approximation.

We may conclude that for the pipeline safety aspects considered in this work, the simpler PR EOS seems sufficient. Its most critical error is the $\approx$ 2–3 bar underprediction of p_{sat}, but as we will see, this is a small error compared to the effects of impurities.

Since PR enables faster and more robust equilibrium calculations, it is used in the next section to further explore the effects of each impurity in a binary mixture with CO_2. Even though this EOS is less accurate, the trends shown with increasing impurity amounts will be similar.

4.2. Effect of impurities

For the four main composition cases (Tab. 1) we see that impurities have a significant impact on the saturation pressure, see Tab. 3. The lower speed of sound at the saturation discontinuity is also influenced, but this is an increase, which makes it safer in terms of running ductile fracture. The effect on the choke temperature seems small.

The effect of each impurity in isolation was studied further. Fig. 6 shows the effect on the phase envelope from 2 mol% of each impurity. As seen, the effect is larger the more volatile the impurity is, with H_2 standing out with a significantly greater effect. We suspect that this is mainly due to the very low molecular weight of H_2 combined with the effects of speed-of-sound. For all these impurities, the effect is to move the bubble line to higher pressures. Fig. 7 shows the effect of impurities on saturation pressure and choke temperature, as a function of increasing impurity amount. As seen, the effect on p_{sat} is significant, and in the direction of increased risk of running ductile fracture. The effect on T_{choke} is not significant for any reasonable impurity amount.

Overall we may summarize the following effects of these impurities:

- The impurities do not have a significant effect on the lowest temperature reached in the decompression in this approximation.
- The impurities give a significant increase of the isentrope saturation pressure. This increases the risk of running ductile fracture.

- The impurities give a significant increase of the cricondenbar, which affects the pipeline pressure required to avoid two-phase flow.
- Impurity levels below 1000 ppm do not have a significant impact on the properties considered here.

We may conclude that for the pipeline safety aspects considered in this work, it is important to consider the presence of impurities in the CO_2. However, if the levels of these impurities are below 1000 ppm, it is likely sufficient to consider the fluid as pure CO_2.

5. Full pipeline decompression simulations

In this section we look at the case studies from Sec. 3 using the full homogeneous equilibrium model described in Sec. 2.1. Herein, we will look at both the short and long time evolution of an industrial size pipeline decompression event using different modelling assumptions.

5.1. Simulation setup

A semi-discrete version of the conservation laws is obtained by using the finite-volume method with the FORCE flux [26]. The temporal integration of the semi-discrete flow equations is performed using the Forward Euler method, with the time-step obeying the Courant–Friedrichs–Lewy (CFL) condition

$$\Delta t = C \frac{\Delta x}{\max\left(|c_{\text{mix}} \pm u|\right)}. \tag{9}$$

Herein, Δx is the length of a computational cell, Δt is the time step, C is the Courant number and c_{mix} is the local speed of sound for the two-phase multi-component mixture. In this work, 200 computational cells and a Courant number of $C = 0.9$ is used in all simulations. A wall boundary condition is applied at the left end of the pipeline, while the right end is a full-bore opening to atmospheric conditions. The heat conduction equation (3) is solved using the finite-volume scheme described by Lund et al. [27], with 10 radial cells.

5.2. Resolution of sound waves

Simulations of the depressurization cases described in Sec. 3 were carried out, with impurities corresponding to compositions #1, #2 and #4 from Tab. 1. This corresponds to pure CO_2, CO_2 with small amounts of impurities and CO_2 with significant amounts of impurities, respectively. The heat transfer and friction terms in Eq. (1) are included in some of the simulations, to illustrate the effect of such terms. The parameters used in the heat transfer model are given in Tab. 2.

Figs. 8 to 10 show snapshots of the pressure and temperature profile at $t = 8\,\text{s}$ after the depressurization for compositions #1, #2 and #4, respectively. The results show significant differences in both the velocity and shape of the predicted decompression wave when

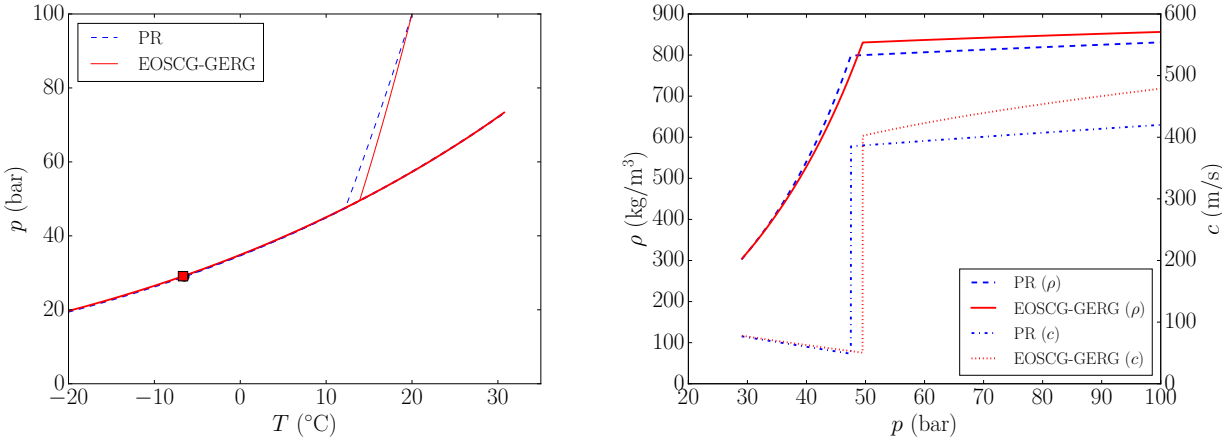

Figure 2: Properties along the isentrope from initial state to choke, with composition #1 (pure CO_2). The evolution in temperature–pressure space is shown together with the two-phase/saturation line in (a). Dots mark the choke point. The evolution of density and speed of sound is shown in (b).

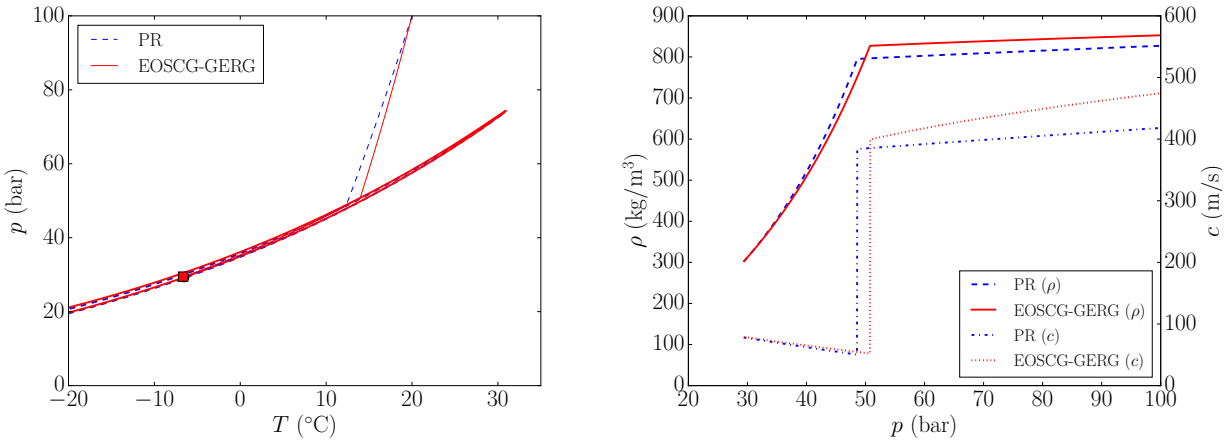

Figure 3: Properties along the isentrope from initial state to choke, with composition #2 (coal power, amine). The evolution in temperature–pressure space is shown together with the two-phase envelope in (a). Dots mark the choke point. The evolution of density and speed of sound is shown in (b).

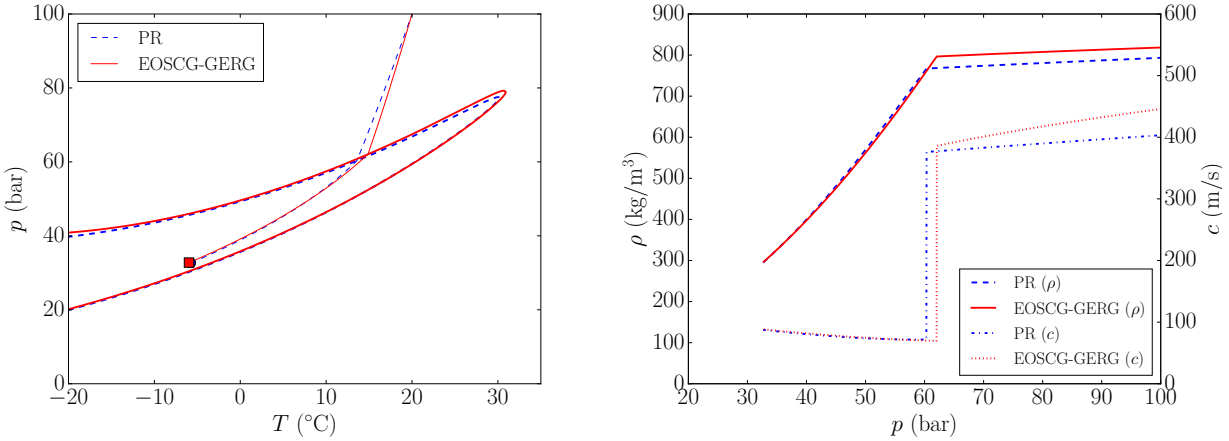

Figure 4: Properties along the isentrope from initial state to choke, with composition #3 (coal power, selexol). The evolution in temperature–pressure space is shown together with the two-phase envelope in (a). Dots mark the choke point. The evolution of density and speed of sound is shown in (b).

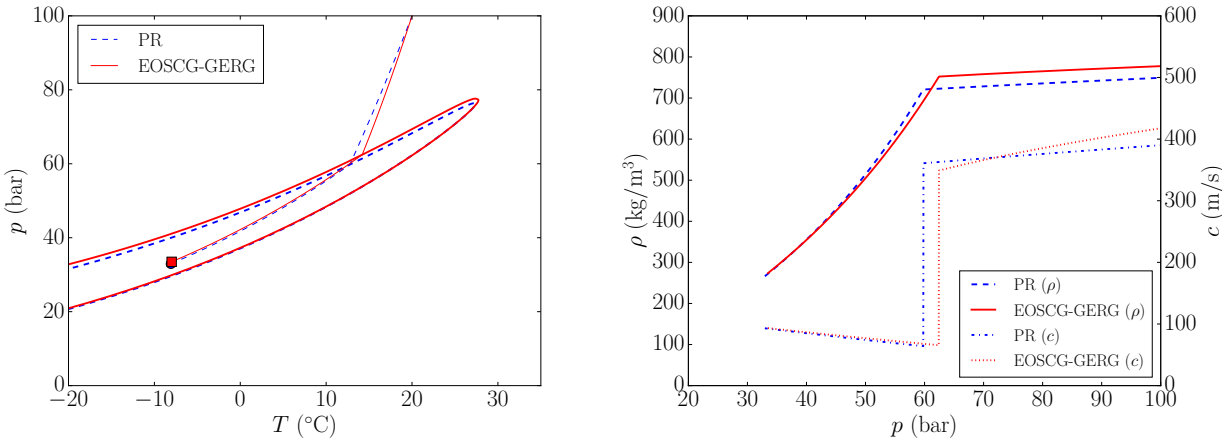

Figure 5: Properties along the isentrope from initial state to choke, with composition #4 (NG processing, amine). The evolution in temperature–pressure space is shown together with the two-phase envelope in (a). Dots mark the choke point. The evolution of density and speed of sound is shown in (b).

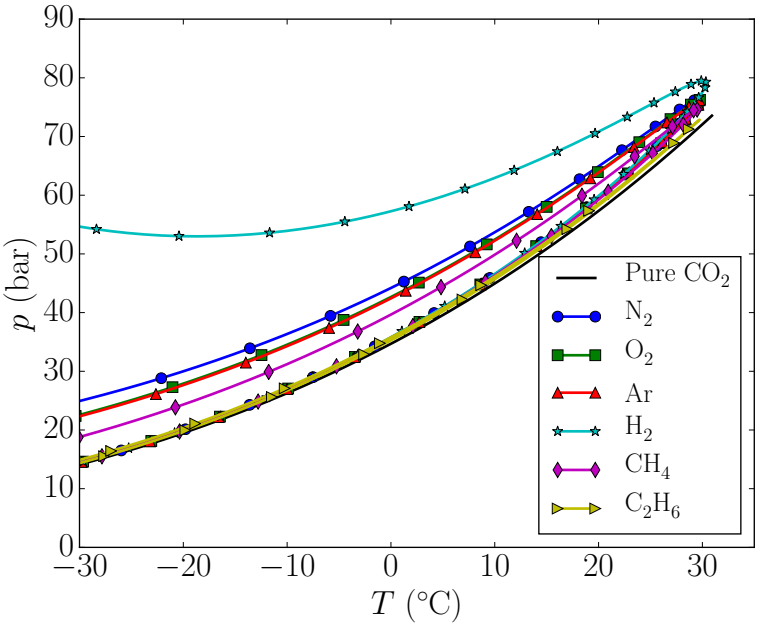

Figure 6: The phase envelopes resulting from 2 mol% of single impurities in CO_2, as compared with pure CO_2. Calculated using the PR EOS.

using an cubic EOS or when ignoring friction and heat transfer. In particular, the pressures are significantly higher than the saturation pressure in the pressure plateau when including friction and heat transfer. This emphasizes the importance of including these effects when predicting running ductile fractures, as the driving force behind these is the pressure difference near the tip of the crack. Also, the choice of EOS can be seen to have a significant effect on the predicted speed of sound, and as a consequence, the propagation of the fast pressure wave.

5.3. Full decompression

Full pipeline decompressions were performed for compositions #2 and #4, corresponding to small and large amounts of impurities, respectively. Here, friction and heat transfer was included in all simulations, and the results using both the Peng–Robinson and the EOSCG-GERG equations of state were compared. Note that since the model does not take into account the solid phase, the decompression case has been chosen in such a way to avoid the triple point temperature of CO_2.

Fig. 11 shows the pressure and temperature evolution near the full-bore opening, as well as the gas volume fraction, for the full decompression event using composition #2. Note that since the pipe is of finite length, there is significantly stronger cooling in the pipeline simulations than what is predicted by the isentropic analysis in Sec. 4. The effect of using accurate thermodynamics (EOSCG-GERG) on the long time evolution is however limited. This is consistent with the results from Sec. 4. There is an isentropic decompression into the

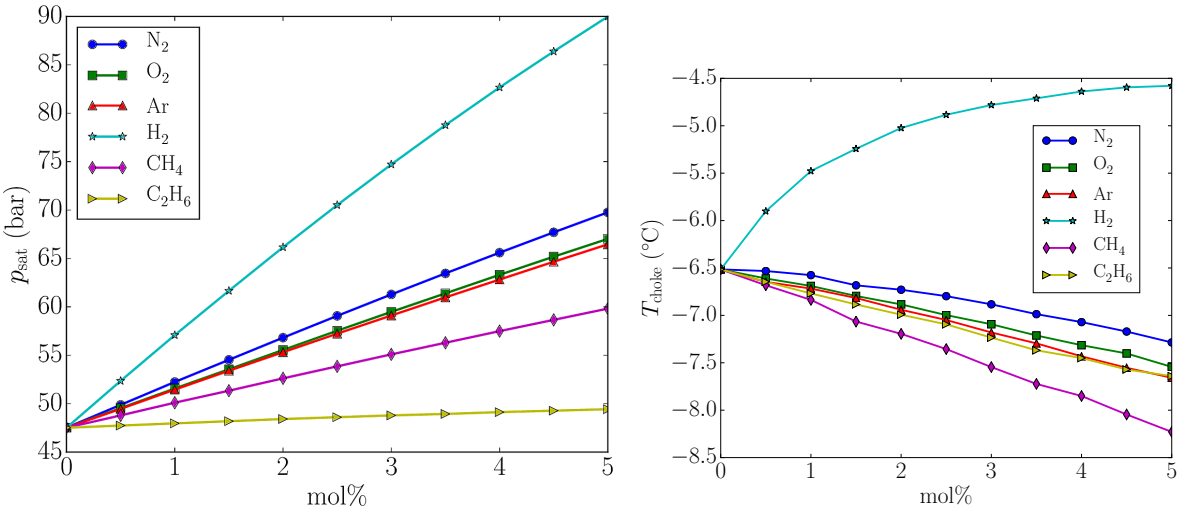

(a) (b)

Figure 7: The effects of single impurities in CO_2 on saturation pressure (a) and choke temperature (b), in the infinite pipe isentropic decompression approximation. Calculated using the PR EOS.

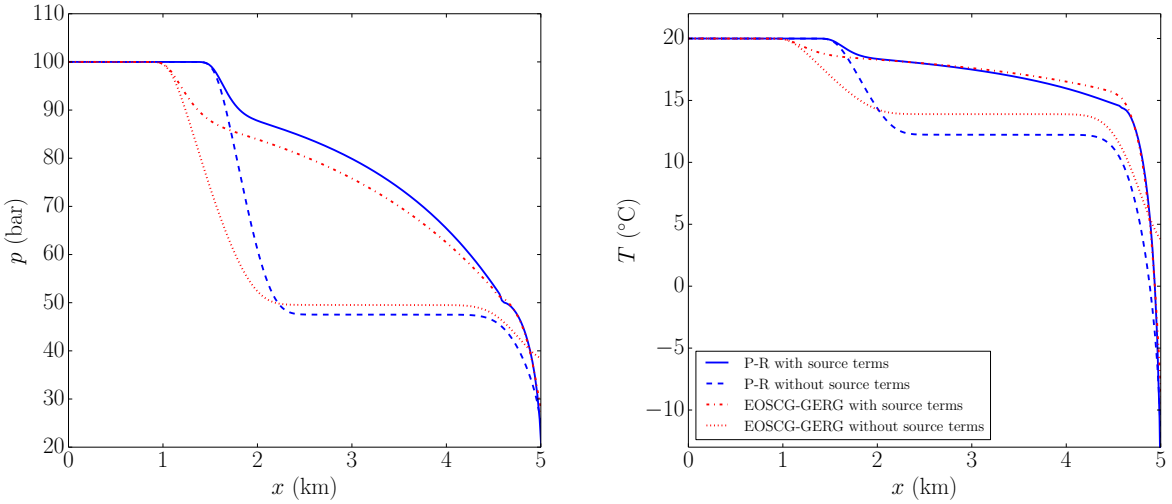

(a) Pressure (b) Temperature

Figure 8: Pressure and temperature at $t = 8$ s using different equations of state and with or without friction and heat transfer. The composition is 100 % CO_2.

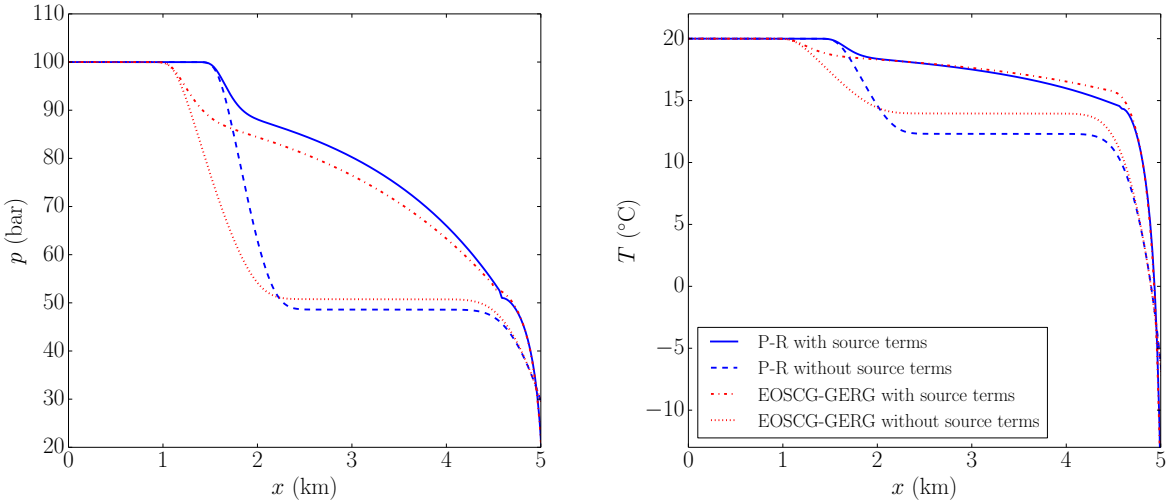

(a) Pressure (b) Temperature

Figure 9: Pressure and temperature at $t = 8$ s using different equations of state and with or without friction and heat transfer. Impurities correspond to composition #2, with 99.77 % CO_2, 0.2 % N_2, 0.02 % O_2 and 0.01 % Ar.

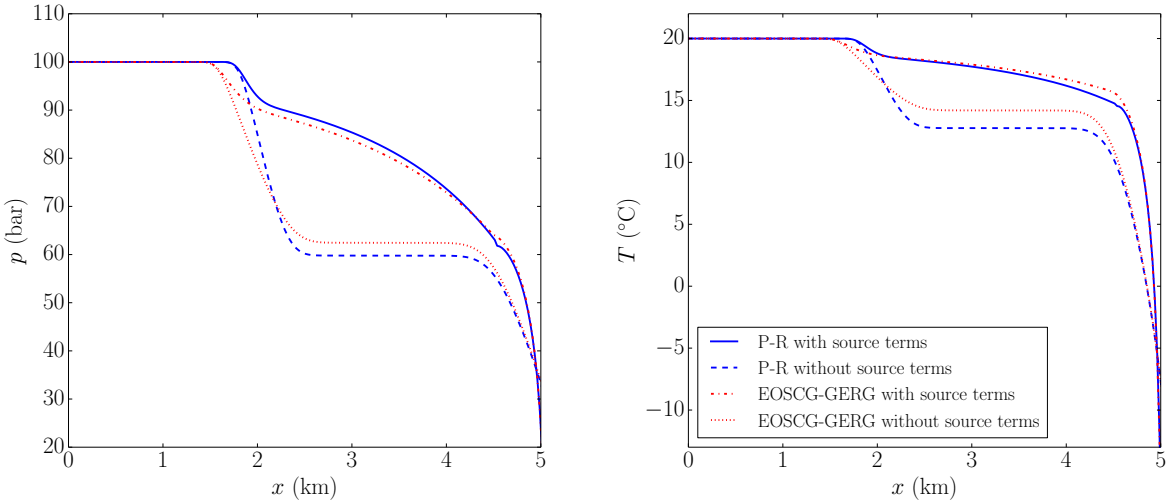

(a) Pressure (b) Temperature

Figure 10: Pressure and temperature at $t = 8$ s using different equations of state and with or without friction and heat transfer. Impurities correspond to composition #4, with 95.0 % CO_2, 4.0 % CH_4, 0.5 % N_2 and 0.5 % C_2H_6.

two-phase region. The temperature will keep decreasing until all the liquid has evaporated. At this point, heat transfer from the surrounding soil will cause a gradual heating of the fluid. These results indicate that the choice of EOS has a smaller effect on the minimum temperature than e.g. heat transfer models and conditions.

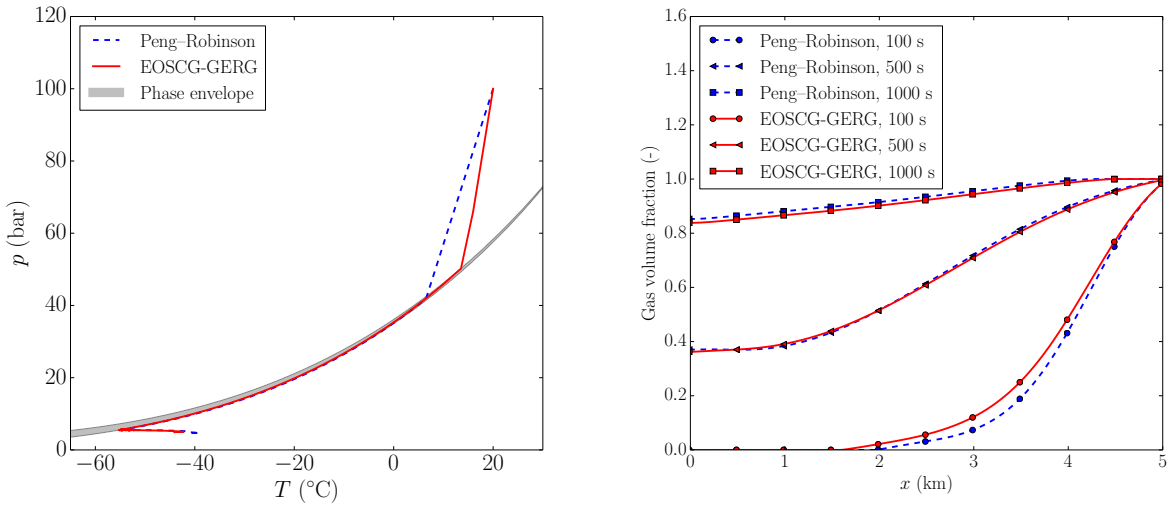

(a) Evolution of pressure and temperature near the full-bore opening.

(b) Gas volume fraction in the pipeline for different times.

Figure 11: The long-time evolution of the depressurization of a 5 km pipeline. Impurities correspond to composition #2, with 99.77 % CO_2, 0.2 % N_2, 0.02 % O_2 and 0.01 % Ar.

Fig. 12 shows the corresponding results for composition #4. Here there is a significant presence of impurities and a wider phase envelope. These results are similar to those seen in Fig. 11: using an accurate EOS has a minimal effect on the long time evolution of the temperature and pressure near the opening. In particular, the predicted minimum temperature is almost identical.

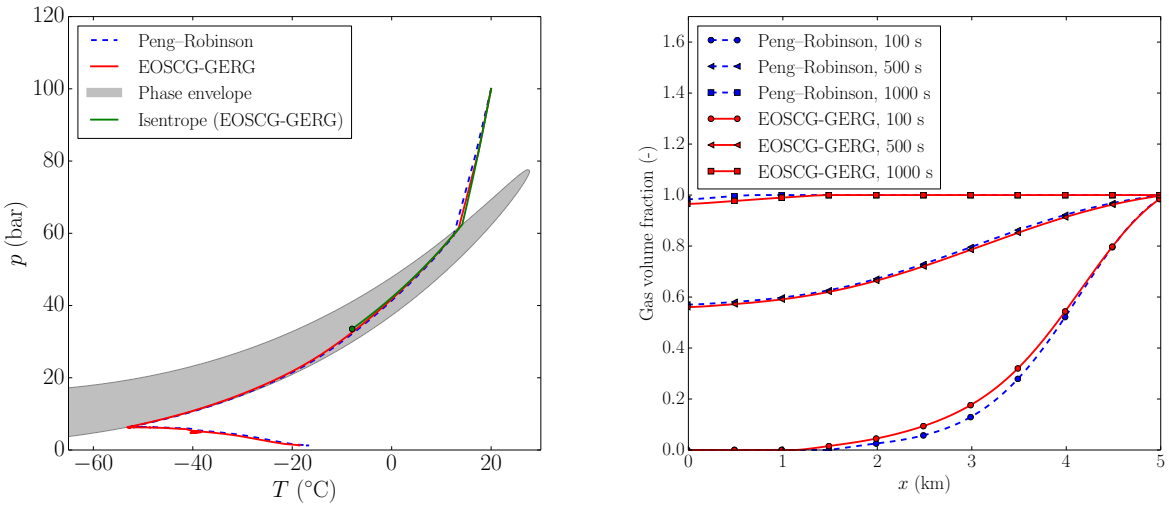

(a) Evolution of pressure and temperature near the full-bore opening.

(b) Gas volume fraction in the pipeline for different times.

Figure 12: The long-time evolution of the depressurization of a 5 km pipeline. Impurities correspond to composition #4, with 95.0 % CO_2, 4.0 % CH_4, 0.5 % N_2 and 0.5 % C_2H_6.

6. Conclusion

We have investigated the temperature and pressure during a depressurization of a CO_2 pipeline, and how they depend on the choice of thermodynamic model and the amount of impurities in the mixture. The depressurization was modelled using two approaches: a purely thermodynamic isentropic calculation, and a flow model including friction and heat transfer. Two equations of state, the Peng–Robinson cubic EOS and the EOSCG–GERG EOS, were used and compared. We considered pure CO_2 and a number of CCS relevant mixtures, as well as a range of binary mixtures with CO_2 and nitrogen, oxygen, argon, hydrogen, methane or ethane.

Two parameters were given special attention: the saturation pressure and the lowest temperature encountered during a depressurization. The former is important due to the implications for running ductile fracture, and it is also related to the necessary operating pressure to avoid two-phase flow in the pipeline. The latter should be predicted correctly in order to stay within the design temperature limits of the pipeline and other equipment, and to avoid the formation of ice and hydrates which could plug the pipeline.

Our results can be summarized as follows:

- The saturation pressure depends significantly on impurities
- The saturation pressure is dependent on the choice of EOS
- The lowest temperature is hardly affected by impurities or choice of EOS

- The lowest temperature is more affected by heat transfer than EOS or impurities

Other important observations include:

- Friction and heat transfer significantly alter the short-term pressure evolution
- The Peng–Robinson EOS underpredicts the liquid speed of sound
- The choice of EOS does not significantly affect the shape of the phase envelope
- The choice of EOS significantly alters the isentrope in the liquid phase
- The cricondenbar increases significantly when impurities are added

Overall, the most important result is that impurities significantly increase the saturation pressure and cricondenbar, which has implications for ductile fractures and the necessary operating pressure. It is also interesting to observe that for safety assessments for pipeline depressurization, the choice of EOS is less important. These results can have important implications for the design of pipelines and the identification of acceptable impurity levels in CO_2 mixtures.

Note that while complex EOSs like EOS-CG and GERG appeared unnecessary for the safety aspects considered in this work, they are absolutely necessary in other contexts such as fiscal metering of normal operation CO_2 transport. This is due to the large error in high pressure liquid density shown in the simpler cubic EOSs such as Peng–Robinson.

Inclusion of a solid phase is a natural extension of this work. This is expected to reduce the outflow rate somewhat, due to a lower speed of sound when the solid phase is in equilibrium with the other phases. Dry-ice may be included using an auxiliary model by e.g. Trusler [19], Jäger et al. [20].

7. Acknowledgement

The research leading to these results has received funding from the European Community's Seventh Framework Programme (FP7-ENERGY-20121-1-2STAGE) under grant agreement no 308809 (The IMPACTS project). The authors acknowledge the project partners and the following funding partners for their contributions: Statoil Petroleum AS, Lundin Norway AS, Gas Natural Fenosa, MAN Diesel & Turbo SE and Vattenfall AB.

References

[1] US DOE, Interagency Task Force on Carbon Capture and Storage, Washington, DC, USA, 2010.

[2] E. de Visser, C. Hendriks, M. Barrio, M. J. Mølnvik, G. de Koeijer, S. Liljemark, Y. Le Gallo, Dynamis CO_2 quality recommendations, International Journal of Greenhouse Gas Control 2 (4) (2008) 478–484. doi:10.1016/j.ijggc.2008.04.006.

[3] J. Capelle, J. Furtado, Z. Azari, S. Jallais, G. Pluvinage, Design based on ductile–brittle transition temperature for API 5L X65 steel used for dense CO2 transport, Engineering Fracture Mechanics 110 (0) (2013) 270 – 280.

[4] E. Aursand, C. Drum, M. Hammer, A. Morin, S. T. Munkejord, H. O. Nordhagen, CO_2pipeline integrity: Comparison of a coupled fluid-structure model and uncoupled two-curve methods, Energy Procedia 51 (2014) 382–391. doi:10.1016/j.egypro.2014.07.045.

[5] NETL, CO_2 impurity design parameters, Tech. Rep. DOE/NETL-341-011212, National Energy Technology Laboratory, USA (Aug. 2013).

[6] P. Aursand, M. Hammer, S. T. Munkejord, Ø. Wilhelmsen, Pipeline transport of CO_2 mixtures: Models for transient simulation, International Journal of Greenhouse Gas Control 15 (2013) 174–185. doi:10.1016/j.ijggc.2013.02.012.

[7] L. Friedel, Improved friction pressure drop correlations for horizontal and vertical two phase pipe flow, in: Proceedings, European Two Phase Flow Group Meeting, Ispra, Italy, 1979, paper E2.

[8] K. E. Gungor, R. H. S. Winterton, Simplified general correlation for saturated flow boiling and comparisons of correlations with data, Chemical Engingeering Research & Design 65 (2) (1987) 148–156.

[9] S. T. Munkejord, M. Hammer, Depressurization of CO_2-rich mixtures in pipes: Two-phase flow modelling and comparison with experiments, International Journal of Greenhouse Gas Control 37 (2015) 398–411. doi:10.1016/j.ijggc.2015.03.029.

[10] D. J. Picard, P. R. Bishnoi, The importance of real-fluid behavior and nonisentropic effects in modeling decompression characteristics of pipeline fluids for application in ductile fracture propagation analysis, Canadian Journal of Chemical Engineering 66 (1) (1988) 3–12. doi:10.1002/cjce.5450660101.

[11] D. Y. Peng, D. B. Robinson, A new two-constant equation of state, Industrial & Engineering Chemistry Fundamentals 15 (1) (1976) 59–64. doi:10.1021/i160057a011.

[12] J. Gernert, R. Span, EOS-CG: An accurate property model for application in CCS processes, in: Proc. Asian Thermophys. Prop. Conf., Beijing, 2010.

[13] R. Span, T. Eckermann, S. Herrig, S. Hielscher, A. Jr, M. Thol, TREND. Thermodynamic reference and engineering data 2.0, lehrstuhl fuer Thermodynamik, Ruhr-Universitaet Bochum (2015).

[14] J. Gernert, R. Span, EOS-CG: A Helmholtz energy mixture model for humid gases and CCS mixtures, Journal of Chemical Thermodynamics 93 (2016) 274–293. doi:10.1016/j.jct.2015.05.015.

[15] O. Kunz, W. Wagner, The GERG-2008 wide-range equation of state for natural gases and other mixtures: An expansion of GERG-2004, Journal of Chemical and Engineering Data 57 (11) (2012) 3032–3091. doi:10.1021/je300655b.

[16] R. Tillner-Roth, Die thermodynamischen Eigenschaften von R152a, R134a und ihren Gemischen: Messungen und Fundamentalgleichungen, Forschungsberichte des Deutschen Ke- und Klimatechnischen Vereins, Nr. 41, 1993.

[17] E. W. Lemmon, A generalized model for the prediction of the thermodynamic properties of mixtures including vapor-liquid equilibrium, Ph.d. dissertation, University of Idaho, Moscow, Idaho, USA (1996).

[18] H. Li, J. Yan, Evaluating cubic equations of state for calculation of vapor liquid equilibrium of CO_2 and CO_2-mixtures for CO_2capture and storage processes, Applied Energy 86 (6) (2009) 826–836. doi:10.1016/j.apenergy.2008.05.018.

[19] J. P. M. Trusler, Equation of state for solid phase I of carbon dioxide valid for temperatures up to 800 K and pressures up to 12 GPa, Journal of Physical and Chemical Reference Data 40 (4), article 043105. doi:10.1063/1.3664915.

[20] A. Jäger, R. Span, Equation of state for solid carbon dioxide based on the Gibbs free energy, Journal of Chemical and Engineering Data 57 (2) (2012) 590–597. doi:10.1021/je2011677.

[21] M. L. Michelsen, State function based flash specifications, Fluid Phase Equilibria 158-160 (1999) 617–626. doi:10.1016/S0378-3812(99)00092-8.

[22] M. Drescher, K. Varholm, S. T. Munkejord, M. Hammer, R. Held, G. de Koeijer, Experiments and modelling of two-phase transient flow during pipeline depressurization of $CO_2$with various N_2compositions, Energy Procedia 63 (2014) 2448–2457. doi:10.1016/j.egypro.2014.11.267.

[23] M. Hammer, Ervik, S. T. Munkejord, Method using a density-energy state function with a reference equation of state for fluid-dynamics simulation of vapor-liquid-solid carbon dioxide, Industrial & Engineering Chemistry Research 52 (29) (2013) 9965–9978. doi:10.1021/ie303516m.

[24] J. F. Ely, H. J. M. Hanley, Prediction of transport properties. 1. Viscosity of fluids and mixtures,

Industrial & Engineering Chemistry Fundamentals 20 (4) (1981) 323–332. doi:10.1021/i100004a004.
[25] J. F. Ely, H. J. M. Hanley, Prediction of transport properties. 2. Thermal conductivity of pure fluids and mixtures, Industrial & Engineering Chemistry Fundamentals 22 (1) (1983) 90–97. doi:10.1021/i100009a016.
[26] E. F. Toro, Riemann solvers and numerical methods for fluid dynamics, 2nd Edition, Springer-Verlag, Berlin, 1999.
[27] H. Lund, M. Torsæter, S. T. Munkejord, Study of thermal variations in wells during CO_2 injection, in: SPE Bergen One Day Seminar, Society of Petroleum Engineers, Bergen, Norway, 2015, paper SPE-173864-MS. doi:0.2118/173864-MS.